A EUROPEAN JOURNAL

CHEMPHYSCHEM

OF CHEMICAL PHYSICS AND PHYSICAL CHEMISTRY

Accepted Article

Title: Intraparticle Diffusional Effects vs. Site Effects on Reaction Pathways in Liquid-Phase Cross Aldol Reactions

Authors: Koushik Ponnuru, Jinesh C Manayil, Hong Je Cho, Wei Fan, Karen Wilson, and Friederike Jentoft

To be cited as: *ChemPhysChem* 10.1002/cphc.201701219

Link to VoR: http://dx.doi.org/10.1002/cphc.201701219

A Journal of

ChemPubSoc Europe

WILEY-VCH

www.chemphyschem.org

10.1002/cphc.201701219

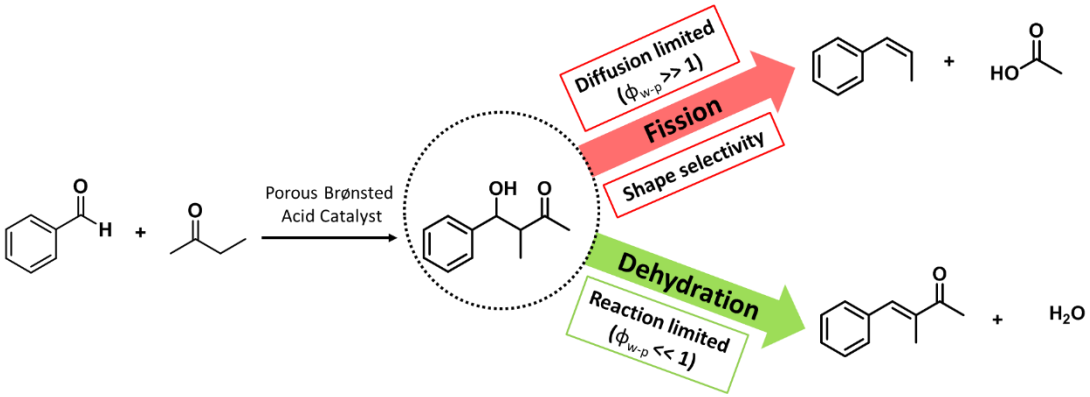

The chemoselectivity towards condensation or fission products in the aldol reaction of benzaldehyde and butanone is directed by using solid acid catalysts, including sulfonic acid-functionalized resins and SBA-15 materials, and β-zeolites, and conditions favoring or preventing diffusion limitation.

Intraparticle Diffusional Effects vs. Site Effects on Reaction Pathways in Liquid-Phase Cross Aldol Reactions

Koushik Ponnuru,[1] Jinesh C. Manayil,[2] Hong Je Cho,[1] Wei Fan,[1] Karen Wilson,[2,3] Friederike C. Jentoft[1,*]

[1]Department of Chemical Engineering, University of Massachusetts, Amherst, 159 Goessmann Laboratory, 686 N Pleasant, Amherst, MA 01003, USA

[2] European Bioenergy Research Institute, Aston University, Birmingham, B4 7ET, UK

[3]New address: School of Science, RMIT University, 124 La Trobe St, Melbourne VIC 3000, Australia.

**Corresponding author email: fcjentoft@umass.edu*

Abstract

Chemo- and regioselectivity in a heterogeneously catalyzed cross aldol reaction were directed by tuning the nature of the sites, textural properties and reaction conditions. Catalysts included sulfonic-acid functionalized resins or SBA-15 with varying particle size or pore diameter, H-BEA zeolites, and Sn-BEA zeotype; conditions were 25 °C to 170 °C in organic media. Benzaldehyde and 2-butanone yielded branched (reaction at -CH_2- of butanone) and linear (reaction at -CH_3) addition and condensation products; and fission of the branched aldol led to β-methyl styrene and acetic acid. Strong acids promoted the dehydration step, and regioselectivity originated from preferred formation of the branched aldol. Both, resins and functionalized SBA-15 materials yielded predominantly the branched condensation product, unless particle morphology or temperature moved the reaction into the diffusion-limited regime, in which case more fission products were formed, corresponding to Wheeler Type II selectivity. For H-form zeolites, fission of the branched aldol competed with dehydration of the linear aldol, possibly because weaker acidity or steric restrictions prevented dehydration of the branched aldol.

Keywords: acid-base catalysis, kinetics, C-C coupling, C-C bond cleavage, transport limitation

1. Introduction

Aldol reactions are versatile C-C bond formation reactions that are widely used in the synthesis of bulk and fine chemicals. For example, higher alcohols and aldehydes are produced by aldol reactions (and subsequent hydrogenation), mostly using liquid catalysts such as caustic soda or acetic acid.[1] Many ingredients in the flavor and fragrance industry are produced via aldol reactions.[2-5] An emerging application of aldol condensation is upgrading of biomass-derived pyrolysis oils for the production of fuels. These oils contain a large fraction of short-chain carbonyl compounds, and aldol condensations have drawn strong interest because they increase carbon chain length while removing oxygen without loss of carbon. For instance, *n*-octane could be produced from the aldol condensation of furfural and acetone followed by hydrodeoxygenation.[6]

For some of these reactions, the regioselective activation of carbonyl compounds with two alpha hydrogens is of significant interest. Regioselectivity control in aldol condensation of unsymmetrical ket-2-ones can be used to preferentially obtain branched or straight carbon chains that are crucial in the synthesis of a variety of aroma chemicals.[2-5] The ability to control the formation of fuel precursors with more or fewer branches would predestine the product for use as gasoline or diesel fuel.

A potentially useful side reaction is the fission of the aldol reaction products which is known to occur during the conversion of acetone to diacetone alcohol and mesityloxide, yielding isobutene and acetic acid. First observed long ago,[7,8] this pathway has drawn attention recently for the sustainable production of isobutene,[9-11] which is a precursor of industrial products such as butyl rubber and ethyl tert-butyl ether.[12] A variety of inorganic solid catalysts have been tested for C−C hydrolytic bond cleavage reactions including mixed metal oxides[9,10,12,13,14] and acidic zeolites[15-19] with efforts focused on catalyst activity and stability. The fission has thus far only been observed in vapor phase conversion at high temperatures (>350 °C), and it is not clear whether these products result from the cleavage of aldol addition or the

cleavage of aldol condensation products. Moreover, little is known about optimizing chemoselectivity for either condensation or fission products.

It is obvious from these examples that it is desirable to steer the regio- and chemoselectivity in aldol reactions. Since homogeneous catalysis is dominant in this area, the known means are those of organic chemistry. Pre-enolization is the most commonly applied method.[20] Variation of the catalyst can also be successful; for example, acids activate hydrogen in the $-CH_2-$ group in butanone whereas bases activate the $-CH_3$ group.[21] Solvents have been reported to significantly affect selectivity in some cases, for example, the enantioselectivity in the Mukayama aldol reaction[22] or the diastereoselectivity in the reaction of *tert*-butyl acetate and 2-phenyl propanal.[23-27] While successful, these methods are not necessarily suitable for large scale processing.

Solid catalysts, in addition to being more easily recoverable than soluble catalysts, offer additional means to improve selectivity. Reactions may be steered by shape selectivity if the reactants and the pores of the catalyst have the same dimensions, or by diffusion limitations in pores if the reactions to be discriminated follow different rate laws and will respond differently to variations in local concentrations. Shape-selective processes are well known in zeolite catalysis and include transition state shape selectivity where formation of an undesired product is precluded, and reactant and product shape selectivity, which can be seen as extreme cases of transport limitation. While the theory on the influence of diffusion limitations on the selectivity in parallel and sequential reactions has been outlined by Wheeler long ago[28] and further expanded by Roberts,[29] practical realizations of these concepts are scarce. Although it is established that intraparticle concentration gradients have a considerable effect on the apparent activity and selectivity of porous catalysts, the effect on activity has received significantly more attention than the effect on selectivity,[30-32] even though selectivity is usually the most important variable in industrial operations. The rate of reaction along the separate pathways in a reaction network can be influenced to

different extents by virtue of the relative abilities of the products and reactants to diffuse through the porous medium.

This paper focuses on selectivities in cross aldol reactions. Butanone and benzaldehyde are chosen as the test reactants to elucidate the reaction network. Butanone as an unsymmetrical ketone allows for regioselective activation at the methyl or methylene group, while benzaldehyde can only act as electrophile. Dehydration is not necessarily immediate,[33] and the aldols may be observed. Fission of the aldol products may produce β-methylstyrene, a chemical intermediate in the manufacture of plasticizers, resins, adhesives and various other valuable polymeric chemicals.[34-36] It will be shown that regioselectivity is diagnostic of the rate-determining step in the aldol condensation[33] and that chemoselectivity is diagnostic of the nature of sites and spatial constraints. Three types of strong Brønsted acidic catalysts are investigated, resin catalysts characterized by mesopores, sulfonic-acid functionalized SBA-15 materials with a combination of meso- and micropores, and zeolites with BEA framework and either only micropores or both meso- and micropores. The influence of transport limitations on product selectivity is also investigated by varying the reaction temperature and by comparing with homogeneous catalysis by benzenesulfonic acid.

2. Experimental section

2.1. Benchmark catalysts

Cross-linked sulfonated polystyrene resins Amberlyst 36 (WET), Dowex 50WX8 (50-100 mesh), Dowex 50WX2 (200 mesh) were obtained from Sigma-Aldrich and served as solid benchmark catalysts, and benzene sulfonic acid (Sigma-Aldrich 97%) served as soluble molecular benchmark catalyst.

2.2. Synthesis and functionalization of SBA-15

2.2.1. Synthesis of SBA-15

SBA-15 materials with different pore architectures were synthesized according to previously reported procedures.[37] Twenty grams of Pluronic P123 (Aldrich) were dissolved in 614 ml of distilled water and 114 ml of 2 M HCl solution by stirring at a temperature of 35 °C. After addition of 46 ml of tetraethylorthosilicate (TEOS), the contents were transferred to a jacketed reactor, combined with a second identically prepared batch, and stirred continuously for 22 h at 35 °C. The resulting gel was divided into four separate batches, which were aged under static conditions in closed polypropylene bottles. Aging time and temperature were varied to obtain samples with different meso and micropore dimensions. The following combinations of times and temperatures were applied: 1 day at 50 °C, 1 day at 80 °C, 2 days at 100 °C, or 7 days at 120 °C. Subsequently, the solid product was retrieved by filtration, washed with DI water and calcined in static air at 550 °C for 5 h. The samples are denoted as SBA-15 (x °C) where x corresponds to the aging temperature during the synthesis of the parent SBA-15.

2.2.2. Propyl sulfonic acid ($PrSO_3H$) functionalization of SBA-15

The synthesis procedure was adapted from Ref. [38] Two grams of calcined SBA-15 (x °C) was stirred with 2.5 ml of 3-mercapto *n*-propyl trimethoxysilane (MPTMS, Sigma) in 60 ml of toluene at a temperature of 130 °C. The suspension was refluxed for 24 h; then the thiol-functionalized solid was retrieved by vacuum filtration, washed with methanol and dried over night at 80 °C. The thiol-functionalized sample was oxidized with H_2O_2 at room temperature for 24 h (30 ml of 33 wt% H_2O_2 per gram of material) to obtain sulfonic acid-functionalized SBA-15. The samples are denoted as $PrSO_3H$/SBA-15 (x °C) where x corresponds to the aging temperature during the synthesis of the parent SBA-15.

2.3. Synthesis of zeolite and zeotype materials

2.3.1. Al-BEA (Fluoride medium)

The synthesis procedure was adapted from Ref. [39] Two separate solutions were first prepared that contained 0.01 g of aluminum powder in 3.06 g of tetraethylammonium hydroxide (TEAOH) (35%, Alfa Aesar) and 10 g of (TEOS) in 8 g of TEAOH, respectively. The two solutions were mixed in a PTFE cup and stirred at room temperature until complete evaporation of water and ethanol. To this mixture, 0.944 ml of hydrofluoric acid (48%, Sigma) was added. The resulting highly viscous gel was heated in a Teflon-lined autoclave and held at a temperature of 140 °C for six days with 30.0-rpm rotation. The obtained solid was washed, dried and calcined at 550 °C in flowing air for 12 h. This sample is denoted as Al-BEA/F^-.

2.3.2. Preparation of Al-BEA (commercial)

The ammonium form of zeolite BEA (CP814E, Si/Al = 12.5) was obtained from Zeolyst. The catalyst was calcined at 550 °C with a ramp rate of 1.0 °C min^{-1} in flowing air for 12 h. This sample is denoted as Al-BEA.

2.3.3. Synthesis of tin-substituted zeotype

The synthesis of Sn-BEA was described in detail in previous reports.[40,41] Briefly, a starting solution was created from tetraethylorthosilicate, TEAOH, tin (IV) chloride hydrate and water and stirred until ethanol formed upon hydrolysis of TEOS had evaporated. A suspension of dealuminated zeolite BEA seeds (corresponding to 4.0 wt.% seed on a silica basis) was added, followed by hydrofluoric acid. The final composition of the synthesis gel was SiO_2: 0.008 SnO_2: 0.54 TEAOH: 0.54 HF: 7.5 H_2O. The gel was heated in an autoclave and held at a temperature of 140 °C for four days with 2.0 rpm rotation. The obtained solid was washed, dried and calcined at 550 °C in flowing air for 12 h.

2.4. Characterization methods

2.4.1. SBA-15

The success of the synthesis was verified with a number of characterization techniques. Low angle XRD patterns were recorded on a Bruker D8 Advance diffractometer fitted with an X'celerator detector and Cu Kα (1.54 Å) source over a 2θ range from 0.3° to 10°. The textural properties were characterized by measuring N_2 adsorption and desorption isotherms at 77 K using a Quantachrome Nova 4000 porosimeter and analyzing the adsorption branches with the BET and BJH methods. The samples were degassed overnight under vacuum at 120 °C before analysis. The sample sulfur content was determined by CHNS analysis on a Thermo Scientific Flash 2000 CHNS-O analyzer. The amount of physisorbed water on the catalyst surface was estimated by performing thermogravimetric analysis (TGA) analysis. A Stanton Redcroft STA780 thermal analyzer was used for this purpose, and 10 mg of sample were heated under N_2 flow (30 ml min^{-1}) at a ramp rate of 10 °C min^{-1} from 40 °C to 800 °C. Surface energies of the catalyst samples were determined by inverse gas chromatography using a Surface Measurement System IGC with IGC controller v1.8 software. Diffuse reflectance infrared Fourier transform spectroscopy (DRIFTS) was performed with a Spectrum 100 spectrometer (PerkinElmer). A Praying Mantis™ diffuse reflectance accessory (DRP-P11, Harrick Scientific) was used with a CHC-CHA-3 environmental chamber (Harrick Scientific). Potassium bromide (Sigma, FT-IR grade) was dried in situ and used to record the background spectrum. The catalysts were diluted in KBr (10 wt%) before the analysis. Scanning electron micrographs of the samples were collected using a Magellan 400 XHR-SEM instrument (FEI) equipped with a field emission gun operated at 3.0 kV. The samples were sputter-coated with platinum before imaging.

2.4.2. Zeolites and metal-substituted zeotypes

Detailed characterization procedures and additional results not repeated here can be found in Ref. [42] The metal content was determined by inductively coupled plasma optical emission spectroscopy (ICP-OES, iCap 6500 Dual view, Thermo Scientific). X-ray diffraction (XRD) patterns of the samples were

recorded on an XRD diffractometer (X'Pert Pro, PANalytical) with Cu Kα radiation operated at an acceleration voltage of 45 kV and a current of 40 mA. N_2 adsorption and desorption isotherms at 77 K were obtained using an automated gas sorption analyzer (Autosorb iQ2, Quantachrome) after the samples were degassed at 300 °C under vacuum for 12 h. Acid site titration by isopropylamine chemisorption with subsequent temperature-programmed desorption (TPD) was performed for Al-BEA and Al-BEA/F^- using a thermogravimetric analyzer with mass spectrometer (TG-MS), specifically an SDT600 TGA system (TA Instruments) equipped with a quadruple mass spectrometer (Extorr XT 300). The number of Brønsted acid sites was determined from the mass loss associated with the evolution of propene, which was identified by MS. DRIFTS and SEM analyses were performed using the same instruments as mentioned in Section 2.4.1.

2.5. Catalytic tests

Batch reactions were performed under autogenous pressure in an oven-dried pressure-resistant glass tube of 15 ml volume equipped with a thermowell (Ace Pressure Tube, Ace Glass 8648-164). Typically, the reaction mixture contained 1.0 M benzaldehyde (Sigma-Aldrich ≥99.5%) and 0.1 M hexadecane in excess 2-butanone (Fisher 99%). The benzaldehyde-to-site ratio was 517 unless otherwise indicated, with sites defined as total moles for homogeneous catalysts, moles of sulfur for functionalized SBA-15, moles of metal for the zeotypes, and moles of acid sites as titrated by isopropylamine chemisorption/TPD for the zeolites, respectively. All solid catalysts were stored in air and used without pre-treatment. The reaction mixture was magnetically stirred in the pressure tube for 20 h at a temperature of 140 °C (unless otherwise indicated) in a temperature-controlled oil bath. The specified reaction temperature was measured by a thermocouple placed in the thermowell. The reaction mixture was centrifuged to remove the solid catalyst before GC analysis.

2.5.1. Reaction product analysis by GC

The reaction products were quantified by using gas chromatography with flame ionization detection (FID); an Agilent 7890B system equipped with an HP-5 capillary column (length 30 m, i.d. 0.32 mm (wide bore), film thickness 0.25 µm) was used. The oven temperature was held at 35 °C for 5 min, ramped at 10 °C min^{-1} to 250 °C, with a hold time of 10 min. The GC injection port was operated at 250 °C in 35:1 split mode with N_2 as the carrier gas at 3 ml min^{-1}, and the injection volume was 0.5 µl. Response factors were calculated using standards of reference compounds or structurally equivalent compounds.[43] Each reaction sample was analyzed at least three times by GC, and the average responses were taken to calculate the conversion, yield, and selectivity. Reported error bars represent standard deviations of repeat catalytic experiments.

In addition, gas chromatography coupled with mass spectrometry (GC-MS) was performed with an Agilent 7890A system (7890 GC/7972 series mass selective detector, HP). Products were identified by using mass spectral library matches and the AMDIS32 software or by measuring reference compounds. The acetic acid in the reaction mixture was determined by derivatizing with trimethylsilyl imidazole (TMSI; Sigma-Aldrich) and subsequent GC-MS analysis as shown in Figure S1.

2.5.2. In-situ ATR-FTIR spectroscopic analysis of the reaction mixture

In addition to GC analysis, the reaction mixture was spectroscopically analyzed in some experiments, to obtain the liquid phase composition with high time resolution. A Mettler-Toledo ReactIR 15 equipped with a DiComp (diamond-composite) attenuated total reflectance (ATR) insertion probe connected by an AgX (silver halide) fiber conduit to a liquid nitrogen-cooled mercury cadmium telluride (MCT) detector was used. The ATR probe was inserted into the Ace pressure tube such that the probe tip remained submerged in the liquid reaction mixture at all times. IR spectra were collected in the wavenumber range from 2000 to 650 cm^{-1} every 60 s with an average of 256 scans per spectrum at a spectral resolution of 4 cm^{-1}. The acquired real-time continuous spectra were exported to the iC Quant™ module to build a

quantitative model for the prediction of absolute concentrations. Baseline correction and solvent subtraction were applied before data processing. Calibration was performed using a univariate model by profiling the characteristic band of benzaldehyde at 827 cm^{-1} from the spectra of reference reaction standards collected at various reaction compositions. The quantitative analysis of the data obtained from the reactIR is explained in detail in Section 1 of the supplementary information.

2.5.3. Calculations

The catalytic performance is reported in terms of benzaldehyde conversion, product selectivity and turnover frequency defined as follows, where *n* is the number of moles and indices *i*, *f*, and *p* mean initial, final and product:

$$\text{Benzaldehyde conversion (\%)} = \left(\frac{n_{Benzaldehyde,i} - n_{Benzaldehyde,f}}{n_{Benzaldehyde,i}} \right) \times 100$$

$$\text{Product yield}_p \text{ (\%)} = \left(\frac{n_p}{n_{Benzaldehyde,i}} \right) \times 100$$

$$\text{Product selectivity}_p \text{ (\%)} = \left(\frac{n_p}{\sum_{products} n_p} \right) \times 100$$

$$\text{Turnover frequency}_{Benzaldehyde} \ (h^{-1}) = \frac{n_{benzaldehyde,i} - n_{benzaldehyde,f}}{time \times n_{active\ sites}}$$

3. Results

3.1. Catalyst characterization

3.1.1. Resin specifications

Properties of the resins as specified by the manufacturer are summarized in Table 1. Exchange capacity was used to calculate the reactant-to-catalyst ratio. Amberlyst 36 is a macroreticular resin with invariably accessible internal surface area, whereas the Dowex products are gel-type resins, which require swelling in a solvent to make the pores accessible.

Table 1 Properties of sulfonated cross-linked polystyrene resins as specified by supplier

Catalyst	Resin type	Exchange capacity, H^+ (eq/l)	Mesh size	Particle size (cm)
Amberlyst 36	Macroreticular	1.95	-	0.030
Dowex 50wx8	Gel	1.70	50-100	0.010
Dowex 50wx2	Gel	0.60	200	0.004
Dowex 50wx2	Gel	0.60	50-100	0.010

3.1.2. Functionalized SBA-15 materials – structure, morphology, texture and composition

The small angle X-ray diffraction patterns and N_2 adsorption isotherms (Figures S2 and S3) confirmed the successful synthesis of the two-dimensional hexagonal lattice (p6mm) of SBA-15 with diffraction peaks corresponding to (100), (110), and (200) reflections.[44] A gradual shift of the (100) reflection towards lower angle was observed with aging temperature, implying an increase in d-spacing. The structure was retained upon functionalization with propyl sulfonic acid groups. The mesopore sizes of the four SBA-15 samples and their functionalized variants ranged from 3.6 to 7.5 nm (Table 2 and Figure S4).

The rod-shaped morphology of the four SBA-15 samples synthesized at different temperatures is evident from Figure 1a-d. The average particle size in these samples is very similar with only slight variations in the length and width of the rods. Typical dimensions were 1 µm long and 0.5 µm wide.

10.1002/cphc.201701219

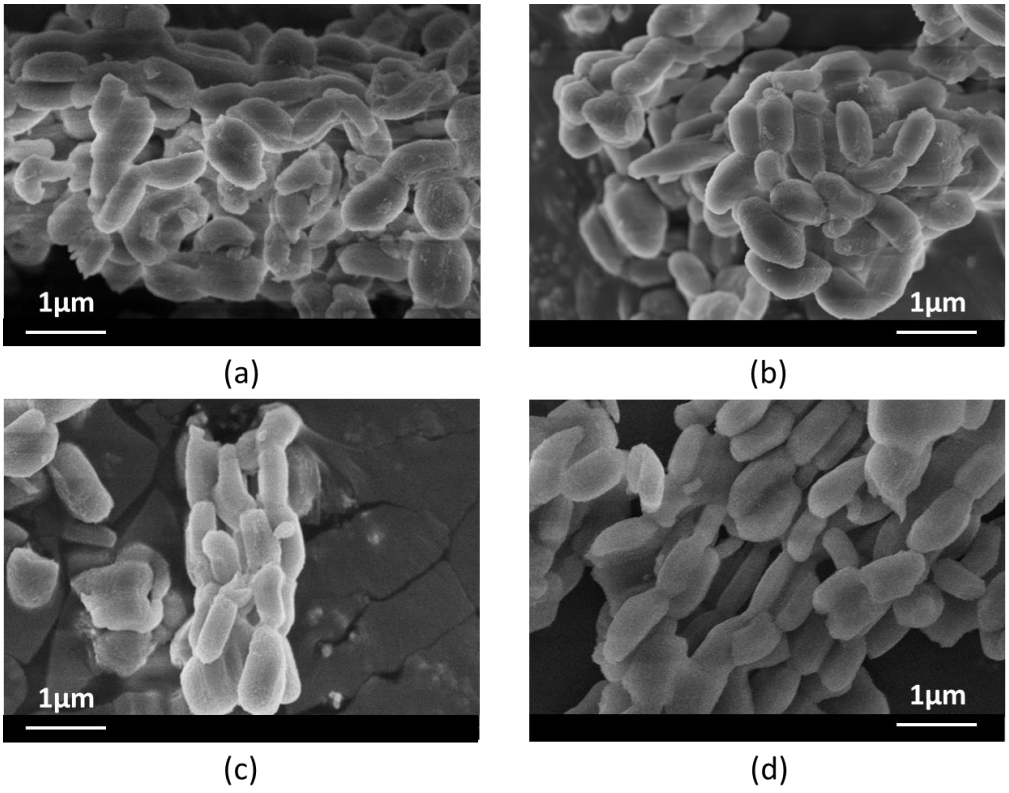

Figure 1. SEM images of (a) SBA-15 (50 °C), (b) SBA-15 (80 °C), (c) SBA-15 (100 °C), and (d) SBA-15 (120 °C).

The textural properties and elemental analysis data of the parent SBA-15 (x °C) series and the functionalized derivatives $PrSO_3H$/SBA-15 (x °C) materials are summarized in Table 2. The mesopore size of the SBA-15 sample increased from 4.1 to 7.5 nm with a concomitant decrease in micropore volume from 0.17 to 0.05 $cm^3\ g^{-1}$ upon increasing the aging temperature from 50 to 120 °C. This reduction in the micropore volume is consistent with previously reported observations for SBA-15.[44] The walls between the mesopores of SBA-15 precursors consist of an interpenetrating network of the P123 template's ethylene oxide chains and silica. Upon calcination, the template is removed, and the micropores are formed in the mesopore walls. The wall thickness can be estimated from the pore diameter and the lattice constant, and the SBA-15 samples with the largest mesopore sizes have thinner walls, resulting in reduced micropore volumes.

No specific trend in BET surface area was observed with aging temperature. The samples aged at lower temperatures (50 °C and 80 °C) were characterized by similar surface areas with an insignificant decrease from 773 $m^2 g^{-1}$ at 50 °C to 759 $m^2 g^{-1}$ at 80 °C. The surface area then increased to 861 $m^2 g^{-1}$ at 100 °C and decreased to 702 $m^2 g^{-1}$ with a further increase in aging temperature to 120 °C. Contrasting trends for BET surface areas were observed in the literature for SBA-15 with increase in aging temperature.[44,45-47] Interestingly, in all these reports, materials aged at a temperature of ≈100 °C always exhibited the highest surface area as in the present investigation. One possibility to rationalize these trends is the dual effect of thinner walls, which imply lower micropore volume but also decreasing density of the material. The BET surface area decreased slightly upon derivatization with $PrSO_3H$ groups for all four SBA-15 samples, whereas there were no clear trends in the behavior of mesopore diameter and mesopore volume. Microporosity, as determined from t-plot analysis, consistently decreased upon introduction of $PrSO_3H$ groups, indicating functionalization of the inner surface of the micropores. In more detail, functionalization significantly reduced micropore volume for samples with small mesopores and high initial micropore volume, and significantly reduced mesopore volume for samples with large mesopores and small initial micropore volume. This result may signify a shift in location of the functional groups from preferably in the micropores to partially in the mesopores.

The sulfur content varied from 0.54 wt% (0.17 mmol g^{-1}) to 0.77 wt% (0.24 mmol g^{-1}) without a recognizable trend (Table 2). Acid sites concentrations were assumed to be equal to sulfur content.

Table 2 Textural properties of functionalized SBA-15 catalysts

Materials	Surface area[a] ($m^2 g^{-1}$)	BJH pore diameter (nm)	Total BJH pore volume ($cm^3 g^{-1}$)	Micropore volume ($cm^3 g^{-1}$)	Micropore Area ($m^2 g^{-1}$)	Pore wall thickness[b], $2R_{wall}$ (nm)	Sulfur content (wt %)	Surface energy (mJ/m^2)	TGA weight loss (50-200 °C) (H_2O, mmol g^{-1})
SBA-15 (50 °C)	773	4.1	0.53	0.17	381	4.48	-	85	0.43
$PrSO_3H$/SBA-15 (50 °C)	699	3.6	0.55	0.10	240	5.19	0.62	-	0.49
SBA-15 (80 °C)	759	4..9	0.76	0.13	305	5.24	-	76	0.35
$PrSO_3H$/SBA-15 (80 °C)	663	4.7	0.77	0.05	115	5.52	0.77	-	0.42
SBA-15 (100 °C)	861	6.4	1.07	0.07	175	3.37	-	74	0.19
$PrSO_3H$/SBA-15 (100 °C)	777	6.2	1.00	0.05	131	3.15	0.62	-	0.34
SBA-15 (120 °C)	702	7.5	1.62	0.05	126	2.50	-	55	0.05
$PrSO_3H$/SBA-15 (120 °C)	460	7.6	1.07	0.02	43	2.39	0.54	-	0.11

[a]BET. [b]Pore wall thickness = d-spacing − pore size; d-spacing calculated from the X-ray diffraction data for (100) plane

3.1.3. Functionalized SBA-15 materials – surface properties

The surface energy values obtained from IGC decreased with increasing aging temperature and mesopore size, indicating that the surface becomes more hydrophobic. Thermogravimetric analysis of the catalyst samples was performed to measure the physisorbed water which is weakly bound to the surface and hence is lost at relatively low temperatures. Therefore, the first weight loss step observed between 50 °C and 150 °C was used to quantify the adsorbed water content of the unfunctionalized SBA-15 series. Hydrophilic properties can be considered to scale with the water content (weight %) of the samples since a H_2O/Si-OH ratio close to 1 has been reported for SBA-15 in the literature.[48] TG traces (Figure S5a) suggest that the sample aged at 120 °C during synthesis is the most hydrophobic in the series as it has the least water loss (1.18%); 50 °C and 80 °C samples have the highest water losses (6.39 and 6.64%), and the 100 °C sample has an intermediate loss (3.89%). A similar hydrophobicity trend was observed for the

functionalized samples. These consistently attracted more water than their unfunctionalized counterparts (Figure S5b and TGA weight loss values in Table 2). This increase in hydrophilicity can be attributed to the polarity of the -SO_3H groups.

DRIFTS analysis was performed to better understand the origins of hydrophobicity of the SBA-15 series surfaces. The spectra were found to be amenable to quantitative interpretation, because the area of the H_2O (ν+δ) combination band at ≈5260 cm^{-1},[48, 49] which is characteristic of physisorbed water, was strictly proportional to the amount of physisorbed water found by TG (Figure 2).

The silanol groups of the synthesized samples were characterized by absorption bands in the 3800-3000 cm^{-1} and 4800-4200 cm^{-1} regions (Figures 3 and S6a,b respectively), which are in agreement with Ref.[49] and can be ascribed to stretching and combinations modes ν(OH) and ν+δ(OH). The ν(OH) bands appearing at ≈3520, 3670, 3710, and 3745 cm^{-1} can be assigned to H-bonded, internal, terminal, and isolated silanol groups, respectively.[50] There was no obvious difference in the OH vibrations between plain and propyl sulfonic acid-functionalized samples. The ν(OH) band of free -SO_3H groups is around 2700-3600 cm^{-1},[51] presumably, strong H-bonding prevented distinction of these vibrations.

10.1002/cphc.201701219

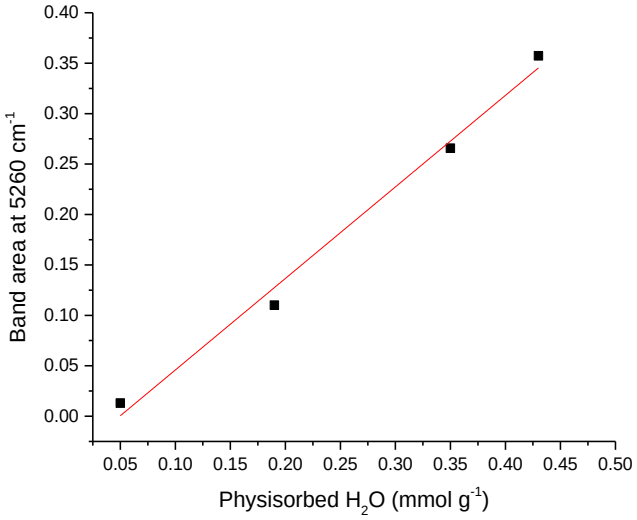

Figure 2. Area of the (ν+δ) H_2O combination band at 5260 cm^{-1} (original spectra in Figure S6a) of sulfonic-acid functionalized SBA-15 (x °C) series versus the concentration of adsorbed water as determined by thermogravimetry (Table 2). DRIFT spectra recorded at 50 °C. Water content decreases with increasing mesopore diameter.

The concentration of unperturbed silanol groups (3745 cm^{-1}) was about equal on all samples before dehydration (Figure 3a). Comparison of spectra recorded before (Figure 3a) and after (Figure 3b) removal of the physisorbed water (disappearance of band at 5260 cm^{-1}, Figure S6b) shows a decrease in H-bonding intensity between 3600 and 3000 cm^{-1} and an increase in isolated silanols at ≈3745 cm^{-1}, indicating physisorption of water on silanol groups.

There was a clear trend towards fewer H-bonded species with increasing aging temperature during synthesis, as seen in Figure 3. This trend was also evident with unfunctionalized SBA-15 samples (not shown). Interacting silanol groups are known to have different reactive properties than isolated silanols, and hydrophilicity is, at least in part, originating from these groups. Presumably, the H-bonding silanol groups are located in micropores; at least there is a rough correlation of the intensity of H-bonded species in Figure 3b with the micropore volumes in Table 2. In summary, DRIFTS data are in agreement with IGC and TG regarding hydrophilicity, as evidenced by H-bonded OH groups and by adsorbed water, respectively.

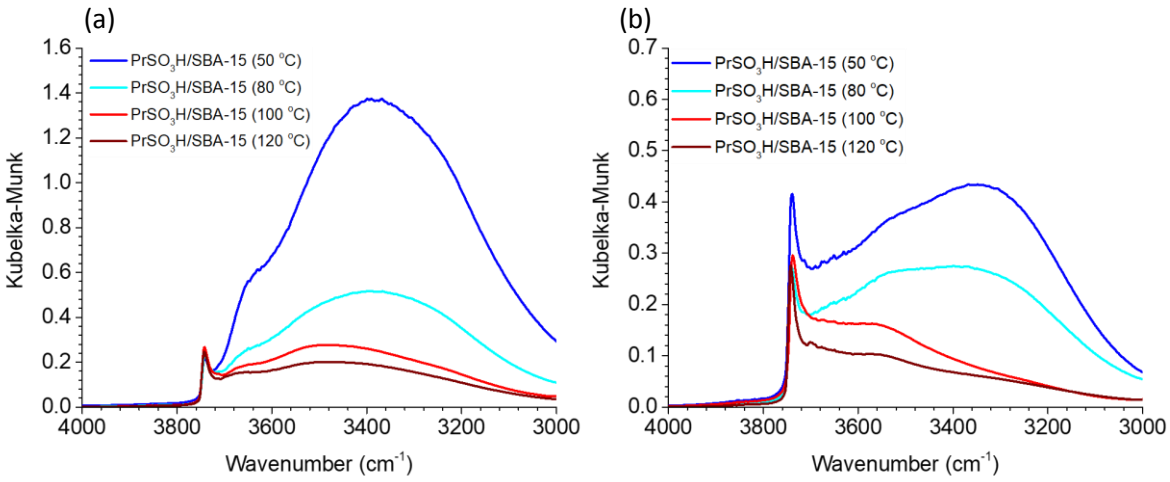

Figure 3. DRIFT spectra of $PrSO_3H$/SBA-15 samples of different aging temperatures in the 4000 – 3000 cm^{-1} region. a) Spectrum of calcined sample recorded at 50 °C. b) Spectrum recorded after heating sample to 200 °C.

3.1.4. Zeolites and metal-substituted zeotypes – structure, composition, morphology and texture

XRD pattern and N_2 adsorption isotherm for Sn-BEA are published in Ref.[40] Data for Al-BEA/F^-, and Al-BEA is shown in Figure S7 of the supplementary information. The XRD patterns of the final solids showed the typical features of the BEA framework with no other crystalline phases being present. N_2 adsorption isotherms measured at a temperature of 77 K indicated that micropore volumes were 0.15–0.17 $cm^3\ g^{-1}$, consistent with the BEA topology (Table 3). Lewis acid site concentrations of zeotype catalysts were assumed to be equal to the metal (tin) content as determined by elemental analysis (ICP-OES), whereas the Brønsted acid site concentrations of the zeolites were determined by isopropylamine TPD.

Table 3 Textural properties and composition of zeotype catalysts

Catalyst	Surface area[a] ($m^2\ g^{-1}$)	Pore diameter (nm)	Total pore volume ($cm^3\ g^{-1}$)	Micropore volume ($cm^3\ g^{-1}$)	Si/metal[b] (mol mol^{-1})	Acid site loading (mmol g^{-1})
Sn-BEA	488	0.75	0.32	0.17	126	0.13[b]
Al-BEA/F^-	528	0.75	0.26	0.16	42.5	0.28[d]
Al-BEA	563	0.75	0.59	0.15	12.5[c]	0.62[d]

[a]BET. [b]Determined from ICP-OES analysis. [c] From the manufacturer (Zeolyst), [d]Isopropylamine TPD.

The SEM image of the Al-BEA in Figure 4a shows agglomeration of the nano-crystallites to larger particles of various sizes with rough appearance and no distinct boundaries, making it difficult to estimate the crystal size from the image. This material was characterized by a Type II isotherm (Figure 4c) and considerably higher total pore volume than micropore volume, consistent with ample void space inside the agglomerates. Diffractograms showed broad reflections consistent with small crystallites. Synthesis of Al-BEA in a fluoride medium resulted in smaller particles, with a diameter of ≈1 μm as seen in Figure 4b. These particles appeared to consist of densely packed, perhaps even intergrown crystallites, consistent with the observed Type I isotherm and the absence of significant amounts of mesopores. Diffractograms were characterized by narrow reflections, indicating large crystallites as observed by others.[39]

3.1.5. Zeolites – surface properties

The strong band at 3735 cm^{-1} in the IR spectrum of Al-BEA (Figure 5) indicates the presence of a large number of isolated silanol groups, which has been correlated to crystal defects and surface hydrophilicity by Camber et al.[52] The decrease in framework Al content by synthesis in fluoride medium produced a sample with notably fewer defects and silanol groups implying a higher surface hydrophobicity in comparison to Al-BEA.

10.1002/cphc.201701219

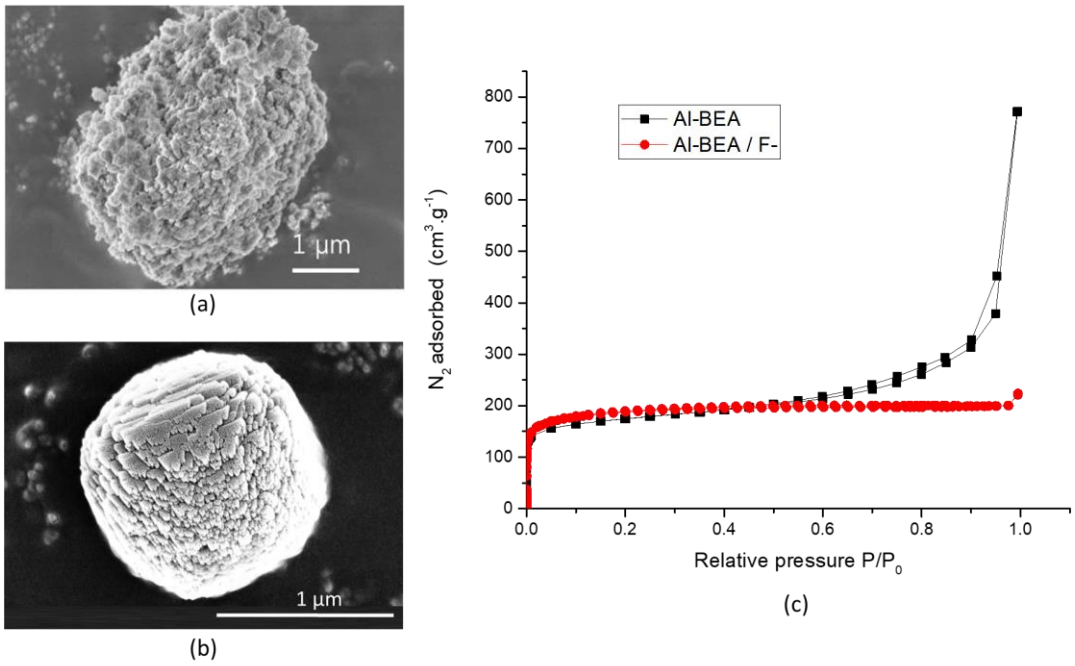

Figure 4. SEM images of (a) Al-BEA, (b) Al-BEA/F^-, and c) N_2 adsorption isotherms of Al-BEA and Al-BEA/F^-.

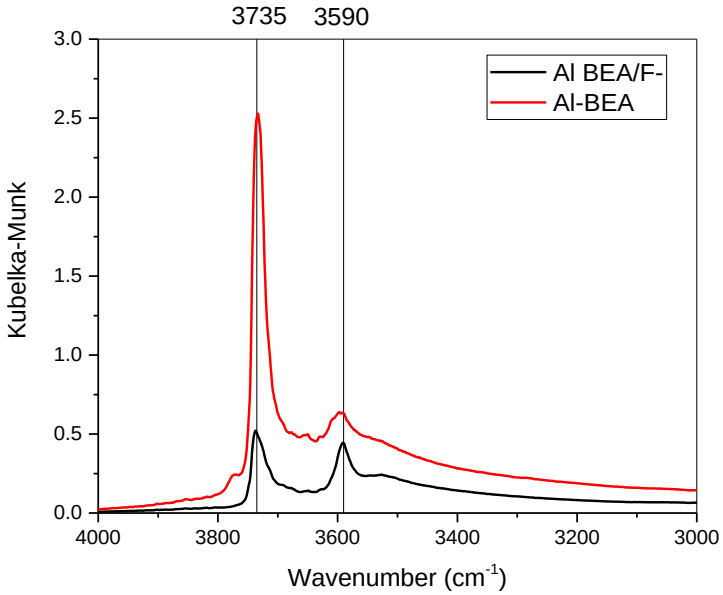

Figure 5. IR spectra of dehydrated zeolite samples recorded at 50 °C.

3.2. Catalytic data

3.2.1. Principal products

Scheme 1 shows the reaction pathways (referred to as Pathways A and B) in the cross-aldol condensation of 2-butanone and benzaldehyde. Reaction at either of the alpha carbons of 2-butanone leads to different addition products (aldols I and II), which can dehydrate to give the condensation products III and IV, respectively. All intermediates and products of the aldol condensation were observed, in varying amounts depending on the catalyst used and reaction conditions.

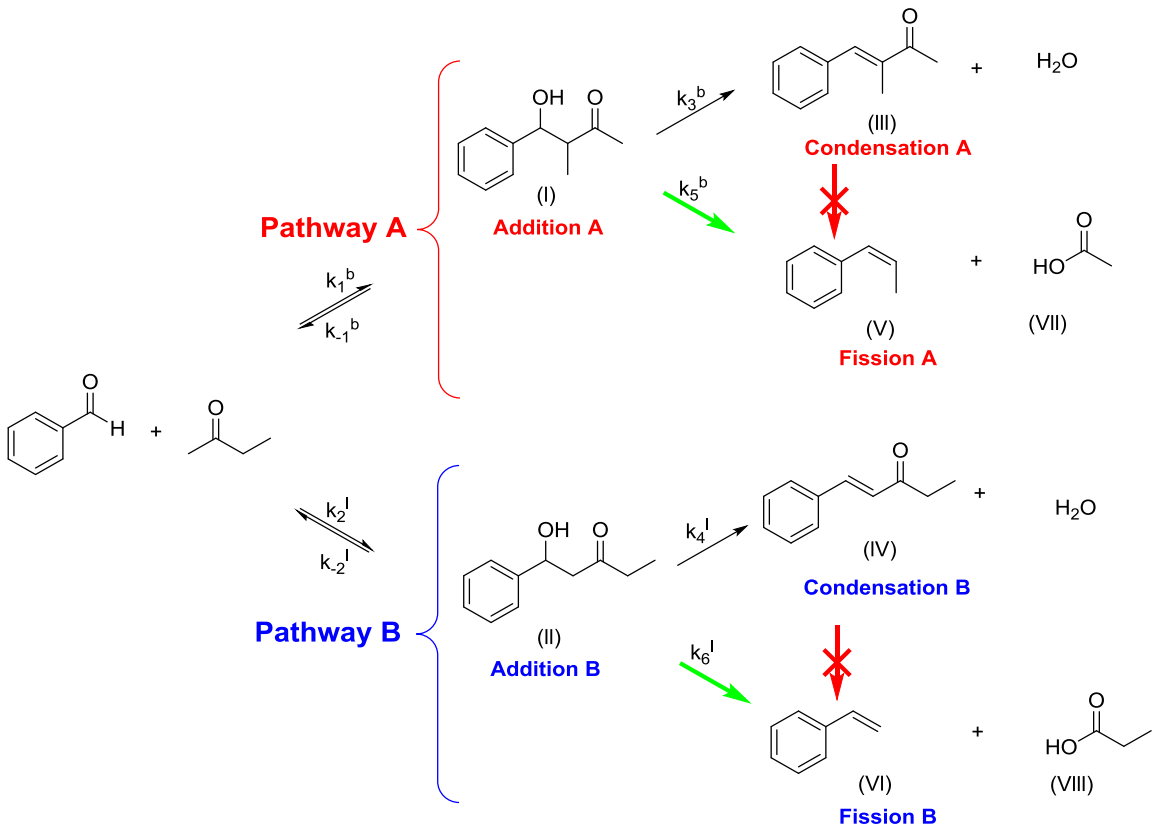

Scheme 1: Reaction network for aldol reaction of butanone with benzaldehyde

Three addition products were chromatographically distinguished. A diastereomeric mixture of erythro- and threo-4-phenyl-3-methyl-butan-4-ol-2-one (referred to collectively as I) indicated condensation at the methylene carbon of the ketone, and 1-phenyl-pentan-1-ol-3-one (II), isomeric with (I), indicated condensation at the methyl carbon of the ketone. The dehydration of the isomeric β-aldols

(I) and (II) resulted in α,β-unsaturated ketones, 3-methyl-4-phenyl-3-buten-2-one (III) and 1-phenyl-1-penten-3-one (IV), respectively.

Previous investigations[33] showed that condensation product yields in excess of 90% are possible, indicating the absence of equilibrium limitations under typical reaction conditions. Further products observed in significant amounts were β-methyl-styrene (V) and acetic acid (VII), formally the result of a C-C bond cleavage in Pathway A. These products will be referred to as fission products, and their formation may be envisioned from the aldol (I) or from the condensation product (III).[9, 10, 13, 15] The corresponding products of Pathway B, styrene (VI) and propionic acid (VIII), were only detected in traces in a few cases and will not be further discussed. The rate constants are represented as *k* and indicated on the arrows of the reaction pathways in Scheme 1. The superscript "*b*" refers to the branched products formed in Pathway A and "*l*" refers to the linear products in Pathway B. The subscript represents the product number formed or disappeared from its corresponding reaction as shown in Scheme 1.

3.2.2. Homogenous catalysis by benzenesulfonic acid

Benzenesulfonic acid was used as a soluble catalyst to provide a benchmark case without diffusion limitation. Independent of the conditions, this catalyst promoted Pathway A, consistent with the regioselectivity reported in the literature. Acid catalysts are known to lead to reaction at the methylene group and formation of the branched addition product.[21, 53] As can be seen in Table 4, Entries 1 to 4, the selectivity to the addition product decreased with conversion whereas the selectivity to the condensation product increased, as is expected for an intermediate product in a series reaction. The regioselectivity of the reaction steadily decreased with increasing temperature (Entries 5-9).

The selectivity toward fission products was significant only at low conversions when aldols can be detected (Entries 1-3), suggesting that cleavage of addition products may yield these products. At high temperatures and high conversions, only traces of fission products were observed (Entries 5-6, 8-9). Selectivities to secondary aldol condensation products were less than 5% at all tested temperatures.

Table 4. Effect of conversion and temperature on product selectivity in excess butanone

Catalyst	Entry	Temp. (°C)	Benzaldehyde Conversion[a] (%)	Addition		Condensation		Fission (%)	ϕ_{w-p}
				A (%)	B (%)	A (%)	B (%)		
Benzene sulfonic acid	1	25	3.5	5.4	0.6	70	11	14	-
	2		34.1	4.85	1.9	72	15	5	-
	3	50	10.5	1.6	0.2	73	13	12	-
	4		50.7	0.3	0.2	83	14	1	-
	5	80	77	0	0.1	84	14	0.3	-
	6	110	79	0	0.2	80	17	0.1	-
	7	140	16	0.7	0	76	16	4	
	8	140	80	0	0.1	78	19	0.2	-
	9	170	78	0	0	71	25	0.3	-
Amberlyst 36	10	50	71	13	0.3	80	6	0.5	0.6
	11	80	54	9	0.9	76	12	2	17
	12	95	62	2	0	81	13	3	32
	13	110	74	1	0.2	77	17	5	54
	14	140	81	0.4	0.1	62	19	17	97
	15	170	70	0.3	0.2	42	19	37	242
Sn-BEA	16	110	26.5	33	2	6	59	0	6
	17	140	31	14	4	9	72	1	19
	18	170	25.5	4	4	9	82	1	79

[a]Benzaldehyde conversion was varied by adjusting the reaction time between 1 to 36 h

3.2.3. Assessment of diffusion limitations

Possible diffusion limitation was evaluated in several ways, by measuring rates as a function of particle size and associated calculations of the Weisz-Prater criterion, and by determining the activation energies. The Weisz-Prater criterion (ϕ_{w-p}) is a critical metric used to determine if a reaction is limited by intraparticle diffusion. The effective diffusivity in the Weisz-Prater criterion incorporates the Knudsen

number λ, which is the ratio of radius of the diffusing product molecule to the radius of the pore. Hence, the criterion accounts for variations in the kinetic diameter depending on the product molecule considered, as well as for variations in pore size when different materials are compared. In general, for $\phi_{w\text{-}p}<<1$, there is no intraparticle concentration gradient and hence the reaction is not limited by diffusion, whereas $\phi_{w\text{-}p}>>1$ indicates strong diffusion limitation. The Weisz-Prater criterion was calculated for all families of catalysts. For the resins, it was assumed that the pore size remains constant. For the SBA-15 series, using mesopore dimensions to evaluate $\phi_{w\text{-}p}$ resulted in a value much smaller than one, suggesting no diffusion limitation in mesopores. Hence, micropore dimensions were used to calculate the Weisz-Prater criterion and these values are reported. For the zeotypes, the effective diffusivities were very conservatively estimated by scaling measured diffusivities[54] rather than by calculating diffusivities from molecular properties and pore dimensions. To evaluate diffusion limitations, the largest species in the reaction network was assessed, and reported dimensions of benzosuberone were used in lieu of the (unknown) dimensions of the addition products. The full calculations are outlined in Section 2 of the supplementary information.

3.2.4. Resin catalysts performance and regimes of diffusion control

The resins are characterized by sulfonic acid groups attached to a benzene ring; thus, their activity would be expected to be in the same range as that of benzenesulfonic acid. With Dowex WX2 200 mesh, characterized by the lowest site density and the smallest particle size, a benzaldehyde turnover frequency (TOF) of 33 h^{-1} was observed versus a TOF of 44 h^{-1} with the free acid (at a temperature of 140 °C in toluene). This result suggests that the resin sites were either slightly less active than benzenesulfonic acid, which could be explained by the *+I* effect of the attached alkyl chain (from the polymer), or were not fully accessible. Like their soluble counterparts, the resins produced predominantly the Pathway A condensation product (Figure 6) and only a small amount of the Pathway B condensation product.

The rate of conversion of benzaldehyde was compared among commercially obtained sulfonated cross-linked polystyrene resin beads with identical $–SO_3H$ groups but different particle sizes (0.074 mm - 0.8 mm). Figure 6 shows similar conversions with increasing number of sites present in the reaction mixture, indicating a decrease in apparent turnover frequency and increasingly severe diffusion limitation. Calculation of the Weisz-Prater criterion for Amberlyst-36 under these conditions gave a value of 156, confirming diffusion limitation. With increasing particle size and more severe transport limitations, the selectivity towards the branched condensation product (III) decreased with an associated increase in the fission product (V) selectivity as shown in Figure 6.

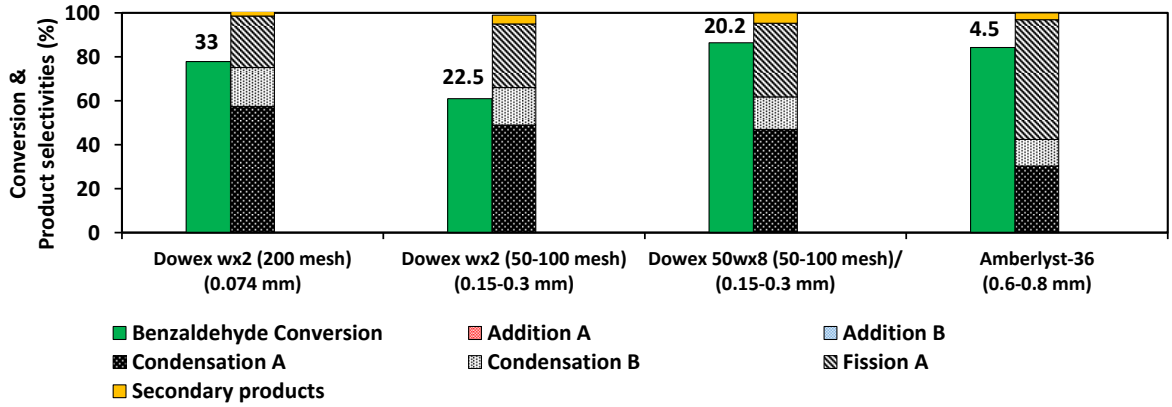

Figure 6. Effect of catalyst particle diameter on product selectivities with sulfonated cross-linked polystyrene resins. Reaction conditions: solvent; toluene, 3 M butanone, 1 M benzaldehyde, 0.1 M hexadecane (internal standard); 140 °C; 10 hours and catalyst mass 50 mg. Site densities are 0.6, 1.7 and 1.95 eq/l for Dowex WX2, Dowex WX8 and Amberlyst-36, respectively. The turnover frequency (h^{-1}) is indicated on the benzaldehyde conversion bars.

To further explore the range of diffusion limitations, the apparent activation energy was determined. The rates measured by in situ ATR-FTIR analysis were used to generate the Arrhenius plot shown in Figure 7. It is evident that there are two different slopes, resulting in different activation energies E_a. The apparent E_a is 48 kJ mol^{-1} in the 50–95 °C range, and 23 kJ mol^{-1} in the 110–140 °C range. The decrease in apparent activation energy with temperature suggests an increased diffusive resistance and further

confirms pore diffusion limitation. The Weisz-Prater criterion also exceeded a value of one at high temperatures (Table 4). Moreover, fission product selectivity increased as temperature and the values for the Weisz-Prater criterion increased, suggesting that the fission products are favored over condensation products as diffusion limitations become more severe.

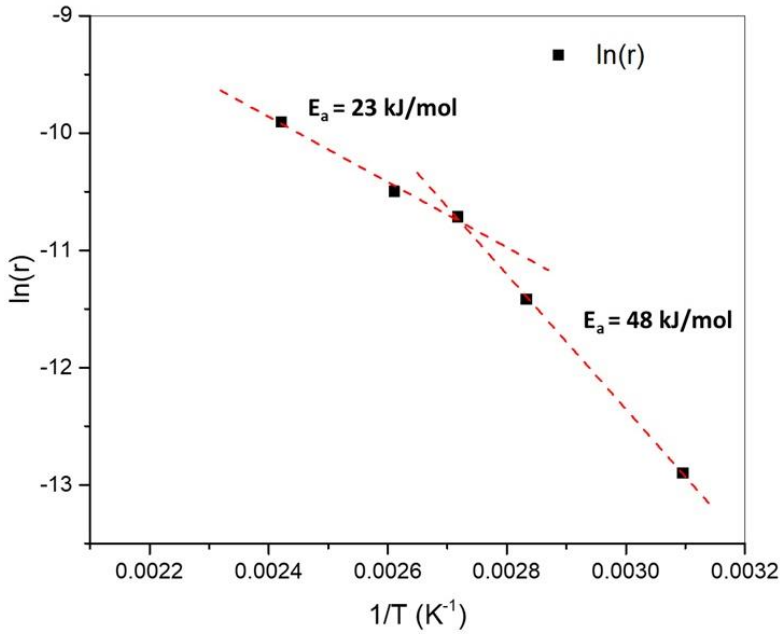

Figure 7. Arrhenius plot of benzaldehyde disappearance rate vs temperature for Amberlyst 36 between 50 °C and 140 °C. Reaction conditions: Excess 2-butanone, 1 M benzaldehyde, 0.1 M hexadecane (internal standard) and catalyst mass 50 mg. The reaction profiles at each temperature are shown in Figure S8.

3.2.5. Reaction pathways investigated using resin catalysts

3.2.5.1. Origin of the fission product

The significant amounts of fission products that were observed with the resins under diffusion control made possible the measurement of selectivities over a wide range of conversions to identify pathways in the reaction network. Cleavage products equivalent to those observed here were observed in other aldol condensations[10,13] and several pathways were formulated, a decomposition of the aldol,[10] or a protolytic or hydrolytic cleavage of the condensation product.[7,8,10,11] To distinguish these possibilities, the Pathway A products were analyzed with one of the benchmark catalysts, Amberlyst 36. Figure 8 shows the

benzaldehyde conversion and the yields of condensation and fission products as a function of reaction time. Benzaldehyde conversion linearly increased with time. Both products yields increased steadily over time, indicating that neither is an intermediate. The yield of the fission product was characterized by a rapid initial rise and moderate growth at long reaction times, while the yield of condensation product was initially low and then grew more significantly over time. These trends suggest parallel formation of these products from the same intermediate (as illustrated in Scheme 1), rather than formation of the fission product from the condensation product.

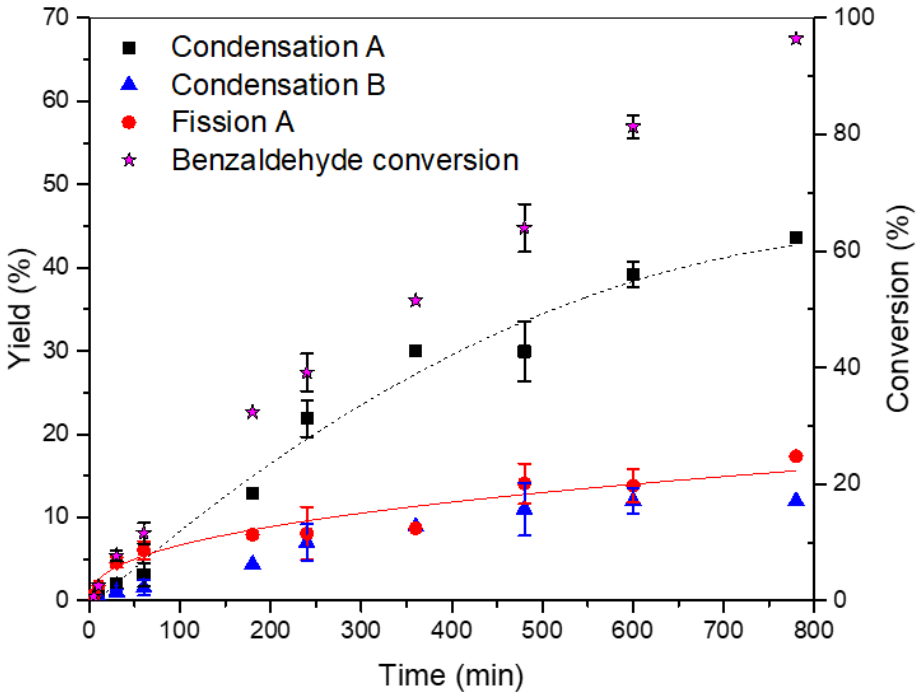

Figure 8. Dependence of product yields in Pathway A on benzaldehyde conversion using Amberlyst 36 in 2-butanone. Reaction conditions: 1 M benzaldehyde, 0.1 M hexadecane (internal standard); excess butanone, 140 °C, catalyst mass 25 mg. Error bars are standard deviations above and below mean obtained from three repetitions of the same test.

It is evident that different rate equations must apply for formation of fission and condensation products if they stem from the same aldol intermediate. The stronger curvature of the fission yield indicates that fission to β-methyl styrene and acetic acid is characterized by a smaller rate constant and a higher order in the aldol than dehydration to the condensation product.

3.2.5.2. Effect of adding water on activity and product selectivity

To further corroborate the formation of the fission product from the aldol, the effect of adding water to the reaction medium prior to the reaction was investigated. Water formed in the condensation step has been proposed to participate in the side reaction to fission products.[9,10,15,55] The addition of water in stoichiometric amounts (1:1 to benzaldehyde) strongly suppressed the rate of benzaldehyde conversion and the rate of formation of the fission products at both 140 °C and 170 °C, as can be seen from the vastly different reaction times (13 h and 4 h at 140 °C, 13 h and 1 h at 170 °C for reactions with and without water respectively) needed to obtain similar conversions in Figure 9.

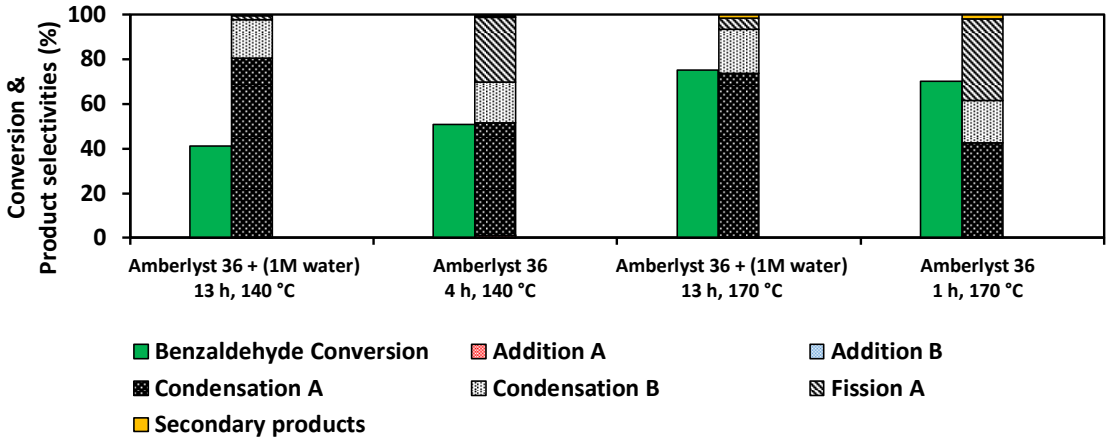

Figure 9. Effect of adding water to the reaction mixture on product selectivities with Amberlyst 36. Reaction conditions: Excess 2-butanone, 1 M benzaldehyde, 0.1 M hexadecane (internal standard), catalyst mass 50 mg, and optionally 1 M water.

3.2.6. Catalytic performance of pore-expanded functionalized SBA-15 materials

The catalyst pore structure, which will have a strong influence on effective diffusivity of reactants and products, is different for the functionalized SBA-15 materials than for the resins. The series of the four $PrSO_3H$/SBA-15 catalysts is characterized by increasing mesopore diameter with concomitantly decreasing micropore volume, and likely by a preferential location of the acid sites in the micropores as deduced by the presence of more H-bonded species (3520 cm^{-1}) in the IR spectrum for the sample with higher micropore volume in Figure 3. The effect of changing the pore architecture on the catalytic performance

is shown in Figure 10. The sites in the samples with larger mesopore diameters were characterized by slightly smaller turnover frequencies, that is, the conversion was slightly lower at equal reactant-to-site ratios and similar reaction times.

Comparison of selectivities at similar conversion provides insights into the reaction pathways leading to different products. All these catalysts preferentially yielded the branched (Pathway A) condensation product, the associated fission products, and undesired secondary aldol condensation products formed through nucleophilic attack of another molecule of benzaldehyde by α,β-unsaturated ketones. The selectivity toward the fission product decreased in the order $PrSO_3H$/SBA-15 (50 °C) > $PrSO_3H$/SBA-15 (80 °C) > $PrSO_3H$/SBA-15 (100 °C) > $PrSO_3H$/SBA-15 (120 °C).

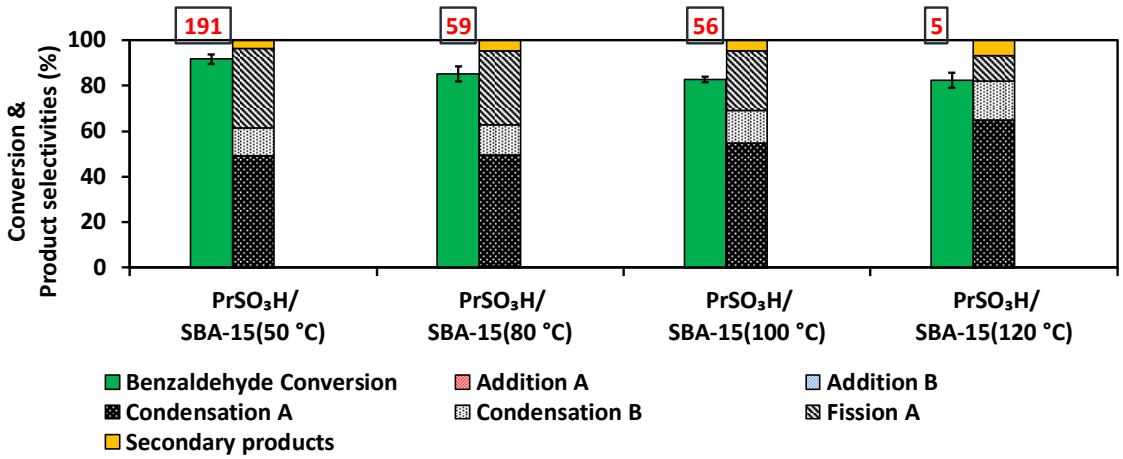

Figure 10. Effect of increasing mesopore diameter and decreasing micropore volume on product selectivity for aldol condensation over $PrSO_3H$/SBA-15. Reaction conditions: 3 M butanone, 1 M benzaldehyde, 0.1 M hexadecane (internal standard); 140 °C, and ratio of benzaldehyde to acid sites of 517:1. Reaction time 8 h. The Weisz-Prater number is indicated on the benzaldehyde conversion bar. Error bars represent one standard deviation above and below mean obtained from three replicate tests. (The error bars for selectivites in stacked bars here are shown in Figure S9.)

$PrSO_3H$/SBA-15 (120 °C) yielded a relatively higher amount of secondary condensation products. The mesopore channels in all samples are wide enough to accommodate these products, and the pore size should not affect the yield. An increase in secondary condensation products with increasing aging

temperature during synthesis could be the result of a higher number of sites in the mesopores space as the micropore space decreases with increasing aging temperature, as discussed in Section 3.1.2.

3.2.7. Catalytic performance of zeotypes and zeolites with BEA structure

Two H-form zeolites with BEA structure were investigated to follow the aldol reaction pathways catalyzed by active sites located exclusively in micropores. The catalytic performance of both commercially obtained Al-BEA and Al-BEA/F^- with reduced connectivity defects synthesized in fluoride medium is presented in Figure 11. These materials differ with respect to the size of the primary microporous crystallites, which are large in Al-BEA/F^-, and with respect to mesoporosity, which is only present in Al-BEA. Al-BEA/F^- synthesized in fluoride medium exhibited much higher activity with a TOF of 40 h^{-1} than the commercially obtained Al-BEA with a TOF of only 8 h^{-1}. The expected product of the aldol condensation reaction in the presence of Brønsted acid sites is the Pathway A condensation product (III), as seen for $PrSO_3H$/SBA-15, but the yield of this product was small for both catalysts Al-BEA and Al-BEA/F^-. Evidently, both aldols I and II were formed, and aldol I fission to β-methyl styrene (favored over dehydration) competed with dehydration of aldol II to the linear condensation product (IV).

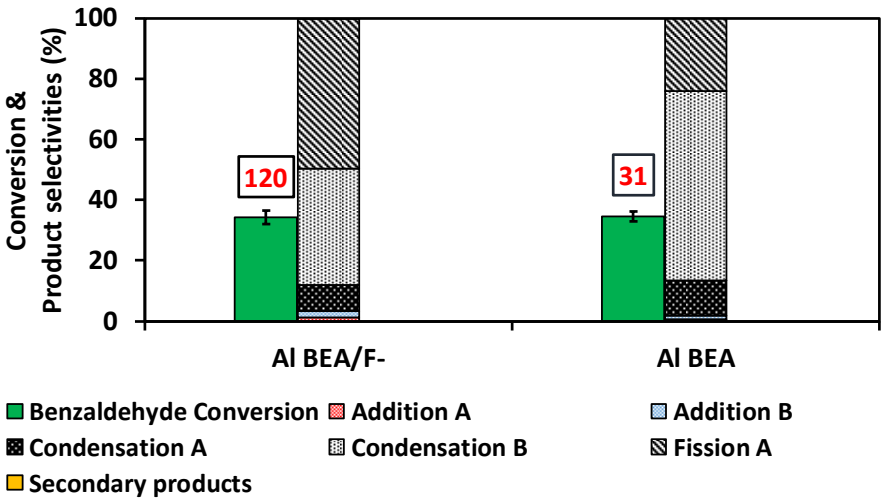

Figure 11. Comparison of activity and product selectivities for Al-BEA/F^- (synthesized in fluoride medium) and Al-BEA. Reaction conditions: Excess butanone, 1 M benzaldehyde, 0.1 M hexadecane (internal standard); 140 °C, and ratio of benzaldehyde to aluminum sites was 385:1. Reaction times were 3 h and 16 h for Al-BEA/F^- and Al-BEA, respectively. The Weisz-Prater number is indicated on the benzaldehyde conversion bar.

Catalytic data for Sn-BEA, which has the same micropore structure as the two H-BEA samples but no strong Brønsted acid sites, can be found in Table 4. In excess butanone, condensation product B was preferentially formed, as reported earlier.[33] Formation of fission products or secondary aldol condensation products was insignificant.

3.2.8. Effect of temperature on selectivity

Product selectivities were examined in a wide range of temperatures across all families of catalysts. The results are shown in Table 4. The effect of temperature on selectivity in the absence of any spatial constraints was explored with benzene sulfonic acid. This catalyst led to fission products only at low conversions (Entries 1-3, 7). At higher temperatures, the catalyst was slightly less selective towards Pathway A condensation products and more selective towards Pathway B condensation products, whereas the formation of fission products was independent of temperature. In contrast, the solid catalyst Amberlyst 36 (Table 4, Entries 10-15, Figure 9) exhibited significantly higher selectivity towards fission with increasing temperature and benzaldehyde conversion. For Sn-BEA, a Lewis acidic zeotype, the fission

product was not observed, not even at elevated temperatures. These results suggest that fission is catalyzed by solid Brønsted acidic catalysts only. Furthermore, Pathway B condensation product (IV) was preferred product at all temperatures with Sn-BEA. Calculation of the Weisz-Prater criterion (last column in Table 4) suggests that at higher temperatures, the heterogeneously catalyzed processes became transport-limited, which in the case of Amberlyst-36 is consistent with the two slopes seen in the Arrhenius plot (Figure 7).

4. Discussion

4.1. Aldol condensation pathway: Relative rates and selectivity depending on catalyst sites

Scheme 1 shows all reaction pathways and names the respective rate constants. Stiles et al.[53] elucidated the relative rates in this particular network by employing the aldol intermediates as reactants. The authors found that the linear aldol (II) of Pathway B dehydrates more easily than the branched aldol (I) of Pathway A. If the dehydration is rate-determining, Pathway B condensation product prevails because the addition steps and their reverse reactions are equilibrated and $k_4^l >> k_3^b$. This scenario is observed when the catalyst is neither a strong base nor a strong acid that would promote dehydration of the aldol. The selectivity seen with Sn-BEA is consistent with its weakly pronounced acid-base properties. In contrast, if dehydration is rapid, then the condensation product selectivity reflects the relative aldol concentrations. The branched aldol A is more easily formed in both acid and base, and in strong acid the addition step is irreversible. Indeed, when aldols are observed in the presence of acid catalysts, mostly at low conversions, then A is always predominant (Table 4). Thus, all sulfonic acid-functionalized materials predominantly produce condensation product A. The behavior of the zeolites H-BEA, which are strong acids but produce the condensation product (IV) of Pathway B, is not explainable with these arguments, and further parameters need to be considered (see below).

4.2. Fission product pathway

By assessing the product selectivities with conversion of Pathway A condensation product (III) and fission product (V) for Amberlyst 36 in Figure 8, it can be concluded that the fission products are not formed from the condensation product (III) but only from aldol (I). If they were to form from (III), the yield of (III) should have significantly decreased with benzaldehyde conversion. However, from Figure 8, the yield of the condensation product (III) increased with benzaldehyde conversion. Therefore, the yields of the fission products depend only on the concentration of the aldol addition products. For a series of irreversible reactions, the expression for maximum concentration of intermediate aldol addition products is given as:[56]

$$\frac{[\text{Addition A}]_{\max}}{[\text{Benzaldehyde}]_0} = \left(\frac{k_1^{\,b}}{k_3^{\,b}}\right)^{\frac{k_3^{\,b}}{k_3^{\,b}-k_1^{\,b}}} \qquad (1)$$

$$\frac{[\text{Addition B}]_{\max}}{[\text{Benzaldehyde}]_0} = \left(\frac{k_2^{\,l}}{k_4^{\,l}}\right)^{\frac{k_4^{\,l}}{k_4^{\,l}-k_2^{\,l}}} \qquad (2)$$

With brackets indicating species concentrations and *k* the rate constants as defined in Scheme 1.

Stiles et al. reported that, in the presence of strong acids, the rate of addition in pathway A is higher than in Pathway B (*i.e.*, $k_1^{b} > k_2^{l}$) and the rate of dehydration is higher compared to the addition step (*i.e.*, $k_3^{b} >> k_1^{b}$ and $k_4^{l} >> k_2^{l}$).[53] These findings suggest that the maximum obtainable concentration of Pathway B aldol (II) will be low as seen from the above equations. Consequently, a poorer yield of Pathway B fission products is expected compared to Pathway A fission products. The same reason can be used to explain the higher selectivity towards fission A observed only at low conversions with homogeneous benzene sulfonic acid where the concentration of aldol intermediate will be high as shown in Table 4 (Entries 1-3, 7).

The fission of the aldol has only been considered by Sun et al.[10] whereas the prevailing mechanism in the literature is the hydrolytic cleavage of the condensation product. However, all literature investigations concern the high temperature vapor phase reactions of the aldol reaction products of acetone, diacetone alcohol and mesityl oxide.

4.3. Directing the chemoselectivity of the reaction towards fission or condensation with sulfonic acid sites

4.3.1. Wheeler Type II selectivity

There is significant evidence that under conditions of diffusion limitation, the sulfonic acid-functionalized materials start catalyzing fission rather than dehydration of aldol (I), deviating from the preferred pathway seen in homogeneous catalysis with benzenesulfonic acid. Various criteria and often more than one indicated diffusion limitation: a Weisz-Prater criterion far above 1 (Figure 10, Table 4, Entries 12-15), an activation energy typical of diffusion control (Figure 7), or a lower turnover frequency (Figure 6 and 9). This shift in selectivity can be understood on the basis of the work of Roberts[29] and Wheeler,[28] who discussed the diffusional resistance effects on reaction selectivity in the case of parallel reactions with a common reactant. The approximate solution derived for several example cases of different individual reaction orders in the asymptotic limit can be applied to the reaction network in this investigation, with aldol (I) as the common reactant. The mathematical formulations of selectivity in both the kinetic and the diffusion-limited regime are presented in Equations 3-5 below:

$$\frac{r_{III}}{r_V} = \frac{k_3^{\,b}[I]^{a_3}}{k_5^{\,l}[I]^{a_5}} \qquad (3)$$

$$\left(\frac{r_{III}}{r_V}\right)_{\text{intrinsic}} = \left(\frac{[III]}{[V]}\right)_{\text{intrinsic}} = \frac{k_3^{\,b}[I]^{a_3}}{k_5^{\,l}[I]^{a_5}} \qquad (4)$$

$$\left(\frac{r_{III}}{r_V}\right)_{\text{observed}} = \left(\frac{[III]}{[V]}\right)_{\text{observed}} = \frac{k_3^{\,b}\int_0^L [I]^{a_3}\,dx}{k_5^{\,l}\int_0^L [I]^{a_5}\,dx} \qquad (5)$$

With *r* the rates of formation, [roman numeral] the concentrations of the species defined in Scheme 1, *a* the reaction orders, and *L* the catalyst particle half width.

From Equations 3-5, it is clear that the product selectivities will be affected only if the kinetic orders of the two competing reactions are different, which is classified as Wheeler Type II selectivity. Figure 8 suggests that the formation of Pathway A fission products proceeds with a higher order compared to dehydration products, and the relative selectivities towards these products, observed in the diffusion-controlled regime are in line with the theoretical predictions.

Mechanistically, the acid-catalyzed dehydration is expected to proceed via an E1 type of mechanism, which would be first order in the aldol. The fission could be an E1 or an E2 mechanism both of which would be first order in the aldol. Observed orders under diffusion limitation may differ from the real orders, making it difficult to align the observed kinetics with a simple mechanistic picture.

4.3.2. Effect of particle size and pore size and possible influence of site cooperativity or hydrophobicity

Using a catalyst with large particles and small pores in conjunction with adequate conditions, that is, operating in the diffusion-limited regime, is equivalent to starting the reaction with high concentration of Addition A, since the effective concentration of Addition A surrounding the site of reaction is increased in both these instances. Thus, the intraparticle diffusion resistance can be used as an advantage to direct

the reaction towards fission pathway and thereby improving the selectivity towards fission A (β-methyl styrene).

The effect of larger particle size is seen well with Amberlyst-36 (Figure 6); the effect of site location in micro- or mesopores is seen with the $PrSO_3H$/SBA-15 samples (Figure 10). The pronounced decrease in micropore volume upon functionalization suggests that micropores are populated with $-SO_3H$ groups. As a result, an increase in selectivity towards Pathway A fission products was observed, consistent with Wheeler Type ll selectivity, with increasing micropore volume in the $PrSO_3H$/SBA-15 series. The calculated Weisz-Prater numbers ($\phi_{w\text{-}p}$) indicated in Table 4 and Figure 10 confirm the association of fission product selectivity with diffusion limitation. Finally, the correlation of fission product selectivity with observable aldol concentrations (Table 4) is consistent with different reaction orders (Wheeler Type II, also seen in Figure 8).

It is worth discussing if an alternative interpretation is viable for these data sets, namely that site cooperativity leads to fission. Site density in the resins in Figure 6 increases concomitantly with particle size and presumably increases in Figure 10 with decreasing SBA-15 mesopore size and increasing micropore volume. It has been reported that cooperativity in sulfonic acid resins is observed at acid loadings as high as those applied here (5.4 mmol g^{-1}).[57] However, cooperativity should not play a role in homogeneous catalysis; nonetheless fission product was formed (Table 4, Entries 1-3, 7), suggesting that cooperativity is not needed.

Another parameter that could affect the selectivity is the overall hydrophobicity. Previous results with a series of sulfonic acid-functionalized SBA-15 samples with different sulfur loadings and with or without octyl co-functionalization demonstrated that the hydrophobicity imparted by the octyl group reduced selectivity toward the fission product. A similar effect could be at play here. As the mesopore size increases with increasing aging temperature, the surface becomes more hydrophobic (Table 2 and DRIFT

spectra in Figures 3 and S5); and water may be rejected by the more hydrophobic surface, favoring dehydration rather than fission. However, this interpretation is in contrast with the results obtained with Al-BEA zeolites (Figure 11), where the fission product was obtained with a higher selectivity for the more hydrophobic Al-BEA/F^- at similar conversion, therefore the observed product selectivity is determined by factors other than surface hydrophobicity of the catalyst.

4.3.3. Effect of water addition

The effect of adding water on the reaction selectivity was studied to understand its influence on the reaction pathways. The detrimental effect of water on the intrinsic reaction rates of the aldol reaction has been extensively discussed in the literature.[57, 58, 59] The reaction rate with Amberlyst 36 in the presence of water was lowered by a factor of ≈3 (Figure 9). At similar benzaldehyde conversion, the selectivity toward fission A reduced to less than 5% even at 170 °C, suggesting that the reaction has shifted from diffusion-controlled regime to the kinetic regime. Another possible explanation for the decrease in reaction rate could be partial hydration of the acid sites on the resin and attenuation of the acid strength to that of H_3O^+ (transition from general to specific acid catalysis) by the additional water in the reaction mixture. In any case, these results demonstrate that continuous removal or addition of water can direct the reaction toward fission or condensation, respectively; although at the expense of rate if water is added.

4.4. Chemoselectivity with Al-BEA Zeolites

The regio- and chemoselectivity of Al-BEA zeolites present a unique situation: both Pathways A and B occur, where A results exclusively in fission products. The significant fraction of Pathway B condensation product (IV) suggests that the dehydration step is rate-determining. The overwhelming fission of aldol (I) rather than its condensation could be the result of lacking acid strength; the deprotonation energy of H-BEA is 1575 kJ mol^{-1},[60] whereas that of benzenesulfonic acid is only 1304 kJ mol^{-1}.[61] In addition, the intermediate aldols (I) and (II) have about the size of the cavities in the BEA framework, making possible

both configurational diffusion-controlled selectivity, which arises from large differences in the diffusivities of differently sized reaction products[28,29] and transition-state shape selectivity, which arises from differences in size and structure of the reaction complexes.[62,63] However, the structure of the intermediates for fission and dehydration are not known. At least, it can be excluded that site cooperativity promotes fission. The site density in commercial Al-BEA is higher than in Al-BEA/F^-, but less fission product is obtained than with Al-BEA/F^-. Another peculiar trend is that the benzaldehyde TOF is higher for Al-BEA/F- than for Al-BEA, although the crystallites of Al-BEA/F^- are much larger. Sites were determined by isopropylamine TPD and should accurately reflect strong Brønsted acid sites; hence, this effect will require further investigation. In any case, H-form zeolites are promising candidate catalysts for promotion of the fission pathway.

5. Conclusions

The reaction network of a cross aldol condensation with an unsymmetrical ketone was elucidated; and the parameters directing regioselectivity and chemoselectivity were investigated by varying surface functionality and texture of the catalyst and the reaction conditions. The aldolization of benzaldehyde and 2-butanone can principally produce a branched (reaction at -CH_2- of butanone) or a linear (reaction at -CH_3) addition product, and corresponding condensation products. Fission of the aldol or the condensation product to an olefin and a carboxylic acid is a possible pathway well known for the aldol reaction of acetone.

It was found that strong soluble or solid acids produce mainly the branched condensation product. This result is consistent with fast dehydration catalyzed by the strong acid, and, consequently, regioselectivity is determined by the preferred formation of the branched aldol. In the absence of strong acid sites, the linear condensation product predominates since dehydration of the respective aldol is facile, consistent with earlier observations in the literature.

Sulfonic acid-functionalized resins and SBA-15, like benzenesulfonic acid, yielded predominantly the branched condensation product, unless transport limitations became significant. The reaction could be moved in and out of the transport limitation regime by varying particle size, pore size, temperature, or water concentration. An interesting shift of selectivity was observed under diffusion limitation, namely the fission of the branched aldol into β-methyl styrene and acetic acid was promoted, which could be explained with Wheeler Type II selectivity.

H-form zeolites presented a unique product distribution; and linear condensation product indicated that fission of the branched aldol competed with dehydration of the linear aldol. Large crystallites of BEA promoted the fission pathway. It is proposed that weaker acidity relative to sulfonic acid or steric restrictions prevented dehydration of the branched aldol.

The findings demonstrate that both regio- and chemoselectivity in solid-catalyzed aldol reactions can be directed by choosing catalyst materials with appropriate surface functionality and texture.

Acknowledgements

This work was, in part, supported by NSF award 1560519. The EPSRC is acknowledged for financial support (EP/K000616/2).

References

[1] K. Weissermel, *Industrial Org. Chem*. John Wiley & Sons, **2008**.
[2] R. E. Naipawer, W. M. Easter U.S. Patent No. 4,052,341, assigned to *Givaudan Corporation,* 4 Oct. **1977**.
[3] R. E. Naipawer U.S. Patent No. 4,696,766, assigned to *Givaudan Corporation,* 29 Sep. **1987**.
[4] S. Abelló, F. Medina, D. Tichit, J. Pérez-Ramírez, J. Sueiras, P. Salagre, Y. Cesteros, *Appl. Catal. B: Environmental*. **2007**, *70*, 577-584.
[5] S. R. Tadepalli, G. K. Tampy, J., U.S. Patent No. 14,283,897, assigned to International Flavors & Fragrances Inc. 22 Dec. **2015**.
[6] R. Ramos, Z. Tišler, O. Kikhtyanin, D. Kubička, *Catal. Sci. Technol.* **2016**, *6*, 1829-1841.
[7] D. V. N. Hardy, *J. Am. Chem. Soc. (Resumed)*. **1938**, 464-468.
[8] S. H. McAllister, W. A. Bailey Jr, C. M. Bouton, *J. Am. Chem. Soc.* **1940**, *62*, 3210-3215.
[9] A. J. Crisci, H. Dou, T. Prasomsri, Y. Román-Leshkov, *ACS Catal*. **2014**, *4*, 4196-4200.
[10] J. Sun, R. A. Baylon, C. Liu, D. Mei, K. J. Martin, P. Venkitasubramanian, Y. Wang*, J. Am. Chem. Soc.* **2016**, *138*, 507-517.
[11] F. Chen, N. Li, S. Li, G. Li, A. Wang, Y. Cong, X. Wang, T. Zhang, *Green Chem*. **2016**, *18*, 5751-5755.

[12] J. Sun, Y. Wang *ACS Catalysis*. **2014**, *4*, 1078-1090.
[13] J. Sun, K. Zhu, F. Gao, C. Wang, J. Liu, C. H. Peden, Y. Wang*, J. Am. Chem. Soc.* **2011**, *133*, 11096-11099.
[14] R. A. Baylon, J. Sun, K. J. Martin, P. Venkitasubramanian, Y. Wang, *Chem. Comm. (Camb)*. **2016**, *52*, 4975-4978.
[15] C. D. Chang, A. J. Silvestri, *J. Catal*. **1977**, *47*, 249-259.
[16] Z. Dolejšek, J. Novakova, V. Bosáček, L. Kubelkova, *Zeolites* **1991**, *11*, 244-247.
[17] G. J. Hutchings, P. Johnston, D. F. Lee, C. D. Williams, *Catal. Lett*. **1993**, *21*, 49-53.
[18] A. Biaglow, J. Sepa, R. Gorte, D. White, *J Catal*. **1995**, *151*, 373-384.
[19] T. Tago, H. Konno, S. Ikeda, S. Yamazaki, W. Ninomiya, Y. Nakasaka, T. Masuda, *Catal. Today*. **2011**, *164*, 158-162.
[20] R. Mahrwald, Aldol Reactions, Springer Netherlands, Dordrecht, **2009**.
[21] M. Beets, H. Van Essen, *Recueil des Travaux Chimiques des Pays-Bas*. **1958**, *77*, 1138-1152.
[22] G. E. Keck, D. Krishnamurthy*, J. Am. Chem. Soc.* **1995**, *117*, 2363-2364.
[23] J. A. Aimetti, M. S. Kellogg, *Tetrahedron Lett*. **1979**, *20*, 3805-3808.
[24] M. R. Mahmoud, H. M. S. El-Kashef, A. M. El-Nady, *Monatsh. Chem.* **1980**, *111*, 657-669.
[25] G. Cainelli, P. Galletti, D. Giacomini, P. Orioli, *Tetrahedron Lett*. **2001**, *42*, 7383-7385.
[26] N. Momiyama, H. Yamamoto*, J. Am. Chem. Soc.* **2004**, *126*, 5360-5361.
[27] L. V. Dashko, D. V. Dmitriev, S. M. Pestov, V. R. Flid, *J. Org. Chem.* **2015**, *50*, 1732-1737.
[28] A. Wheeler, *Adv. Catal.* **1951**, *3*, 249-327.
[29] G. W. Roberts*, Chem. Eng. Sci.* **1972**, *27*, 1409-1420.
[30] M. F. Simpson, J. Wei, S. Sundaresan*, Ind. Eng. Chem. Res.* **1996**, *35*, 3861-3873.
[31] Z. Xu, K. Chuang*, Chem. Eng. Sci.* **1997**, *52*, 3011-3017.
[32] C. Ercan, F. M. Dautzenberg, C. Y. Yeh, H. E. Barner*, Ind. Eng. Chem. Res.* **1998**, *37*, 1724-1728.
[33] K. Ponnuru, J. C. Manayil, H. J. Cho, A. Osatiashtiani, W. Fan, K. Wilson, F. C. Jentoft, *Mol. Catal.* in press. **2017**.
[34] P. O. Powers, *Rubber Chem. Technol.* **1963**, *36*, 1542-1570.
[35] M. Ralph, U.S. Patent No. 3551365 29 Dec. **1970**, assigned to *Matalon Ralph.*
[36] D. Chundury, U.S. Patent No. 07,945,511, 11 Jan. **1994**, assigned to *Ferro Corporation*.
[37] J. P. Dacquin, A. F. Lee, C. Pirez, K. Wilson, *Chem. Comm. (Camb)*. **2012**, *48*, 212-214.
[38] J. C. Manayil, V. C. dos Santos, F. C. Jentoft, M. Granollers Mesa, A. F. Lee, K. Wilson, *ChemCatChem*. **2017**, *9*, 2231-2238.
[39] M. A. Camblor, A. Corma, S. Valencia, *J. Mater. Chem*. **1998**, *8*, 2137-2145.
[40] C. C. Chang, H. J. Cho, J. Yu, R. J. Gorte, J. Gulbinski, P. Dauenhauer, W. Fan, *Green Chem.* **2016**, *18*, 1368-1376.
[41] H. J. Cho, L. Ren, V. Vattipalli, Y.-H. Yeh, N. Gould, B. Xu, R. J. Gorte, R. Lobo, P. J. Dauenhauer, M. Tsapatsis, W. Fan, *ChemCatChem*. **2017**, *9*, 398-402.
[42] H. J. Cho, P. Dornath, W. Fan, *ACS Catal*. **2014**, *4*, 2029-2037.
[43] K. Schofield, *Prog. Energy Combust. Sci.* **2008**, *34*, 330-350.
[44] V. Vattipalli, X. Qi, P. J. Dauenhauer, W. Fan, *Chem. Mater.* **2016**, *28*, 7852-7863.
[45] A. Deryło-Marczewska, A. W. Marczewski, I. Skrzypek, S. Pikus, M. Kozak *Appl. Surf. Sci*. **2005**, *252*, 625-632.
[46] A. Sousa, E. M. B. Sousa *J. Non-Cryst. Solids.* **2006**, *352*, 3451-3456.
[47] A. Sousa, K. C. Souza, S. C. Reis, R. G. Sousa, D. Windmöller, J. C. Machado, E. M. B. Sousa *J. Non-Cryst. Solids*. **2008**, *354*, 4800-4805.
[48] J. P. Gallas, J.-M. Goupil, A. Vimont, J.-C. Lavalley, B. Gil, J. P. Gilson, O. Miserque, *Langmuir* **2009**, *25*, 5825-5834.
[49] A. Burneau, J. Gallas, A. Legrand *Vibrational spectroscopies. John Wiley, Chichester*. **1998**, 147-234.

[50] B. Morrow, I. Cody, L. S. Lee, *J. Phys. Chem*. **1976**, *80*, 2761-2767.
[51] E. Kolvari, N. Koukabi, M. M. Hosseini, M. Vahidian, E. Ghobadi, *RSC Adv*. **2016**, *6*, 7419-7425.
[52] M. Camblor, A. Corma, S. Iborra, S. Miquel, J. Primo, S. Valencia, *J. Catal*. **1997**, *172*, 76-84.
[53] M. Stiles, D. Wolf, G. V. Hudson, *J. Am. Chem. Soc.* **1959**, *81*, 628-632.
[54] P. M. Lima, C. V. Gonçalves, C. L. Cavalcante Jr, D. Cardoso, *Micropor. Mesopor. Mat*. **2008**, *116*, 352-357.
[55] L. K. Freidlin, V. Sharf, *Russ. Chem. Bull.* **1958**, *7*, 1220-1226.
[56] O. Levenspiel, Chemical Reaction Engineering, 3rd Edition. **1998**, P55.
[57] S. Koujout, D. R. Brown, *Catal. Lett*. **2004**, *98*, 195-202.
[58] E. du Toit, W. Nicol, *Appl. Catal., A* **2004**, *277*, 219-225.
[59] Y. S. Mahajan, R. S. Kamath, P. S. Kumbhar, S. M. Mahajani*, Ind. Eng. Chem. Res.* **2008**, *47*, 25-33.
[60] A. J. Jones, E. Iglesia, *ACS Catal*. **2015**, *5*, 5741-5755.
[61] S. N. Ivanov, N. I. Giricheva, T. V. Nurkevich, M. S. Fedorov*, Russ. J. Phys. Chem. A* **2014**, *88*, 661-666.
[62] D. Chen, K. Moljord, T. Fuglerud, A. Holmen*, Micropor. Mesopor. Mat.* **1999**, *29*, 191-203.
[63] L. A. Clark, M. Sierka, J. Sauer*, J. Am. Chem. Soc.* **2004**, *126*, 936-947.